



**HAL**  
open science

## Communication Magnetoresistance and structural characterization of electrospun $\text{La}_{1-x}\text{Sr}_x\text{MnO}_3$ nanowire network fabrics with $x = 0.2$

Thomas Karwoth, Lin Zeng, Michael Rudolf Koblichka, Uwe Hartmann, Crosby S Chang, Thomas Hauet, Jian-Min Li

► **To cite this version:**

Thomas Karwoth, Lin Zeng, Michael Rudolf Koblichka, Uwe Hartmann, Crosby S Chang, et al.. Communication Magnetoresistance and structural characterization of electrospun  $\text{La}_{1-x}\text{Sr}_x\text{MnO}_3$  nanowire network fabrics with  $x = 0.2$ . Solid State Communications, 2019, 10.1016/j.ssc.2018.12.015 . hal-02444166

**HAL Id: hal-02444166**

**<https://hal.science/hal-02444166>**

Submitted on 23 Jan 2020

**HAL** is a multi-disciplinary open access archive for the deposit and dissemination of scientific research documents, whether they are published or not. The documents may come from teaching and research institutions in France or abroad, or from public or private research centers.

L'archive ouverte pluridisciplinaire **HAL**, est destinée au dépôt et à la diffusion de documents scientifiques de niveau recherche, publiés ou non, émanant des établissements d'enseignement et de recherche français ou étrangers, des laboratoires publics ou privés.

# Magnetoresistance and structural characterization of electrospun $\text{La}_{1-x}\text{Sr}_x\text{MnO}_3$ nanowire network fabrics with $x = 0.2$

Thomas Karwoth<sup>a</sup>, Xian Lin Zeng<sup>a</sup>, Michael R. Koblischka<sup>a,\*,1</sup>, Uwe Hartmann<sup>a</sup>, Crosby Chang<sup>b</sup>, Thomas Hauet<sup>b</sup>, Jian-Min Li<sup>c</sup>

<sup>a</sup>Institute of Experimental Physics, Saarland University, Campus C 6 3, 66123 Saarbrücken, Germany

<sup>b</sup>Institut Jean Lamour, UMR CNRS 7198, Université de Lorraine, 54011 Nancy, France

<sup>c</sup>Department of Physics, Zhejiang University, Hangzhou, 310027, People's Republic of China

---

## ABSTRACT

Nonwoven nanowire network fabrics of the material class  $\text{La}_{1-x}\text{Sr}_x\text{MnO}_3$  (LSMO) with  $x = 0.2$  were fabricated employing a sol-gel-process via electrospinning and a subsequent thermal treatment process based on thermal gravity analysis results. Investigations by means of scanning electron microscopy revealed an average diameter of the resulting nanowires of around 230 nm and a length of more than 100  $\mu\text{m}$ . The chemical phases of the samples have been confirmed via X-Ray diffraction. The nanowires are polycrystalline with an average grain size of about 25 nm obtained from transmission electron microscopy. Analyses of the electronic transportation properties and of the magnetoresistive (MR) effects of the nanowire samples were carried out by a four probe measurement inside a bath cryostat in fields up to 10 T. Measurements of magnetization in the temperature range  $2\text{ K} < T < 350\text{ K}$  reveal the Curie temperature (325 K) and are compared to magnetic thermogravimetric data. Magnetization loops  $M(H)$  at room temperature and 4.2 K were carried out revealing the soft magnetic character of the nanowires.

---

## 1. Introduction

Nanowires of functional oxide materials may exhibit different physics as compared to their bulk counterparts due to size effects and the one-dimensional characteristics [1]. In the case of  $\text{La}_{1-x}\text{Sr}_x\text{MnO}_3$  (LSMO), exhibiting the colossal magnetoresistance (CMR) effect, the small wire diameter and the resulting grain size in the low nanometer range may also have a strong effect on the magnetoresistance [2,3].

The magnetoresistance (MR) is discussed in the literature for two different regimes, the low-field MR (LFMR) and the high-field MR (HFMR). The origin of the LFMR is still unclear. Effects contributing are tunnel magnetoresistance (TMR) among grains [4], and spin dependent scattering at interfaces as in giant magnetoresistance (GMR) granular films [5,6]. In Refs. [7,8], it was pointed out that the LFMR can be raised to about 30% for grains with a diameter of around 400 nm and a further reduction of the grain size does not lead to a further increase of the LFMR, and, inversely, the HFMR rises when reducing the grain size. Indications [9,10] have been found that the HFMR becomes larger for samples having low Curie temperature,  $T_C$ . This was confirmed recently in Ref. [11]. The reason for this behavior is ascribed to the presence of a

nonferromagnetic surface layer of few nanometer thickness at the LSMO grains.

In the present contribution, we have fabricated nanowire network fabrics of LSMO with  $x = 0.2$  by means of the electrospinning technique, representing a new class of magnetic material. Electrospinning [12–14] is common for the fabrication of organic polymer nanostructures, but can be modified by employing different precursors to deliver inorganic compounds. Up to now, only a small number of reports are dealing with magnetic nanostructures prepared in this way [14–18]. The resulting LSMO nanowires are of polycrystalline nature with a high aspect ratio (the length of the nanowires is in the 100  $\mu\text{m}$  range, and the diameter is  $\sim 230\text{ nm}$ ). The LSMO grains have nanometric dimensions of  $\sim 25\text{ nm}$ , and the nanowires show numerous interconnects between each other which, together with the GBs between the LSMO grains within the nanowire itself, can further increase the interface effects and thus, enhance the tunneling transport across these interfaces. Furthermore, the present electrospun nanowire network fabrics do not have a substrate which may provide additional strain effects on the nanowires [19,20]. Therefore, we may expect interesting new physical properties of this new class of magnetic material. In order

to achieve a better understanding of the transport properties of the electrospun LSMO nanowire network fabrics, we performed electric and magnetic characterization together with a thorough microstructure analysis including scanning electron microscopy (SEM) and transmission electron microscopy (TEM).

## 2. Experimental procedures

The electrospinning precursor is prepared by dissolving La, Sr, and Mn acetates in PVA (high molecular weight polyvinyl alcohol). The PVA is slowly added to the acetate solution with a mass ratio of 2.5:1.5. This solution is stirred at 80 °C for 2 h, and then spun into cohering nanofibers by electrospinning. To remove the organic compounds and to form the desired LSMO phase, the sample is subsequently heat treated in a lab furnace. An additional oxygenation process is required to obtain the correct phase composition. Further details about the electrospinning process of these nanowires are given elsewhere [21,22].

The constituent phases of the samples were determined by means of a high-resolution automated RINT2200 X-ray powder diffractometer, using Cu-K $\alpha$  radiation generated at 40 kV and a current of 40 mA. The average grain size estimated from the XRD result is about 14.6 nm. For electric measurements, the nanowire network sample is directly laid on two Cu wires (50  $\mu$ m diameter), forming a 'bridge' structure and electrically connected by silver paint as shown in the inset to Fig. 6 below due to the high fragility of the ceramic sheet. The upper two legs from different Cu wires are chosen as current links while the lower two ones are chosen as voltage links. Since each current link is connected with a voltage link, the resulting configuration is a 'pseudo' four-point connection instead of individual four point contact. Considering the high resistivity of the sample (in M $\Omega$  scale), the accuracy of the resulting resistance is nevertheless highly reliable.

The magnetization of the nanowire networks were measured using a superconducting quantum interference device (SQUID) magnetometer (Quantum Design MPMS3) with  $\pm$  7 T magnetic field applied perpendicular to the sample surface, using a piece of the nanowire network with a size of 14.86 mm<sup>2</sup>.

Magnetic thermogravimetric analysis (MTGA) was measured employing a homebuilt apparatus with a maximum field of 0.4 T (applied perpendicular to the sample surface).

The magnetoresistance was measured in a 10/12 T bath cryostat (Oxford Instruments Teslatron) with a Keithley source meter (model 2400) as a current source, and the voltage was recorded using a Keithley 2001 voltmeter.

## 3. Results and discussion

### 3.1. Microstructure

In Fig. 1, the XRD data of our nanowire network fabric sample is given. The experimental data were indexed using the PDF-card #50-0308. All the reference peak positions are indicated along with the experimental data. According to this analysis, the sample shows a pure LSCO phase with tetragonal lattice structure. No additional phases can be seen, however, one has to assume that some carbon is still residing in the grain boundaries since the sample is obtained via a burnout of the polymer fiber. EDX spectroscopy is applied to the sample fixed on an aluminium holder as shown in the lower graph of Fig. 1. Table 1 presents the results from three different sample positions. As result, the sample exhibits a similar element distribution as La: Sr: Mn = 0.185: 0.780: 1.034, which is close to the target ratio of La: Sr: Mn = 0.2: 0.8: 1. Thus, we consider the sample to have a relatively uniform element distribution within the La<sub>0.8</sub>Sr<sub>0.2</sub>MnO<sub>3</sub> phase. This is rational as the nanowire fabric sample is electrospun from a uniform sol-gel solution, and the sample is further heat-treated at 650 °C, where the La<sub>1-x</sub>Sr<sub>x</sub>MnO<sub>3</sub> phase is considered as the stable phase dominating this

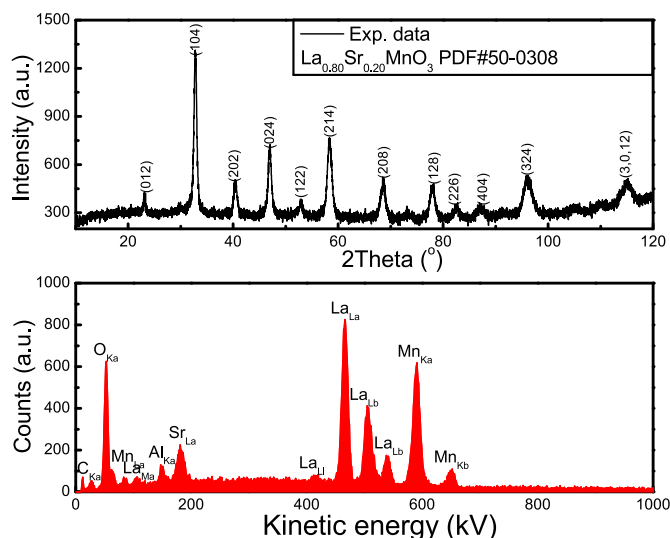


Fig. 1. X-ray analysis of the LSMO nanowire network sample, with the peaks defined by the standard PDF card #50-0308 (upper) and the EDAX spectrum of the same sample on Aluminium holder (lower).

Table 1

EDAX analysis of the LSMO ( $x = 0.2$ ) sample at three different positions.

Element	O K	Sr L	La L	Mn K
Area 1	44.69%	4.74%	21.91%	27.66%
Area 2	48.24%	4.92%	20.93%	25.91%
Area 3	49.85%	4.64%	19.58%	25.93%

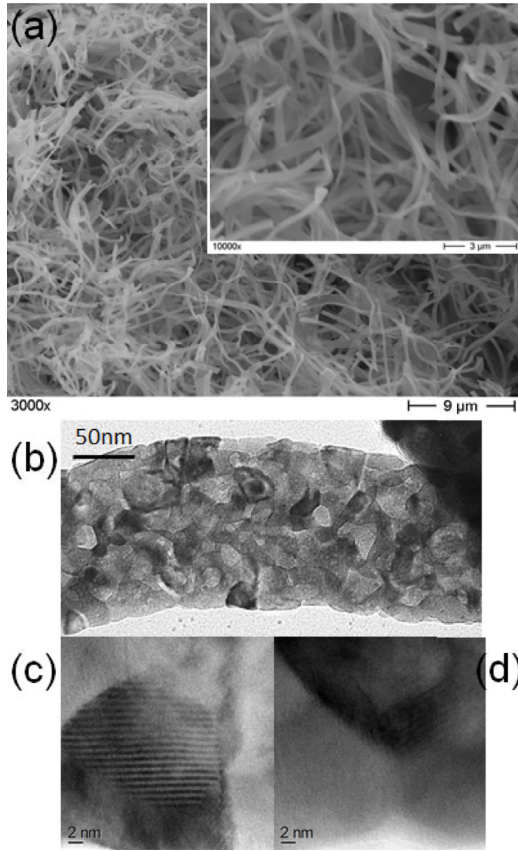
temperature regime.

Fig. 2 presents an SEM image (a) with magnification 3000 $\times$  together with an inset with higher magnification (10000 $\times$ ). Here, the long lengths of the individual nanowires up to the 100  $\mu$ m range are obvious. At higher magnification, the large number of interconnects between the individual nanowires within the sample gets visible. These interconnects, formed during the final heat treatment step, are essential for the current flow through the entire sample perimeter. Fig. 2 (b) shows a TEM image of an individual nanowire piece. An individual nanowire is formed of a stack of several LSMO grains. The grains within the nanowire are randomly oriented with high-angle grain boundaries between them, which becomes even more obvious in the high-resolution TEM images of individual grains in Fig. 2 (c) and (d), where lattice fringes can be seen. These images reveal grain boundary widths of  $\sim$  5 nm.

Fig. 3 (a,b) present the analysis of the nanowire diameters and the LSMO grain size determined from several SEM and TEM images. The graph of the nanowire diameter reveals an average diameter of 227.8 nm as determined by a Gauss fit to the experimental data. The grain size determined from TEM images varies between 10 and 32 nm with an average of 24.8 nm. Analysing the XRD data shown on Fig. 1, the grain sizes estimated from the FWHM of the three strongest peaks (104), (024) and (214) are 15.2 nm, 17.6 nm, and 12.6 nm respectively. The larger average grain size obtained from the TEM data indicates that there are multiply connected domains in the sample.

### 3.2. Magnetization data

In Fig. 4 (a) and (b), the temperature dependence of the magnetic properties of the LSMO sample were measured using SQUID magnetometry and by employing magnetic thermogravimetric analysis (MTGA). In (a), the  $M(T)$  curve in the temperature range 2 K <  $T$  < 350 K measured after zero-field cooling of the sample is presented. The Curie temperature,  $T_C$ , is determined from the fits indicated to be 325.5 K,



**Fig. 2.** (a) SEM image of the nanowire network at  $3000\times$  magnification. The inset shows a higher magnification ( $10000\times$ ) illustrating the numerous interconnects between the long nanowires. (b) gives a TEM image of an individual LSMO nanowire revealing the polycrystalline, randomly-oriented grain structure, and (c,d) show high-resolution TEM images of individual LSMO grains and their boundaries.

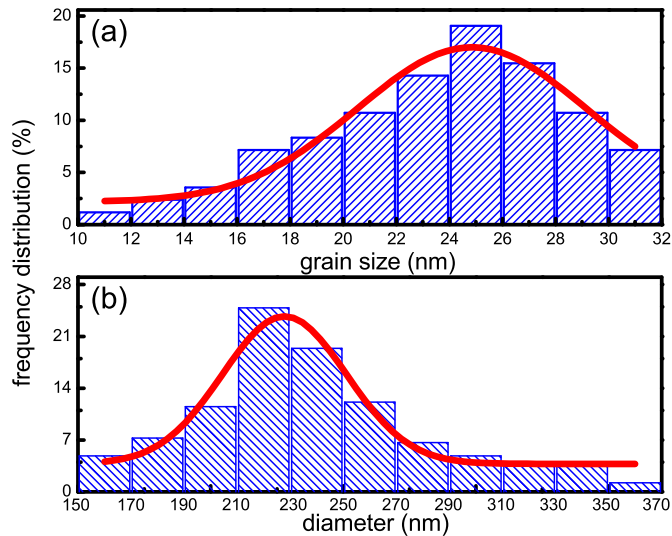


**Fig. 3.** Statistics of the nanowire diameter and the grain size. The average nanowire diameter is determined by a Gauss fit to be  $227.8\text{ nm}$ , the average grain size is  $24.8\text{ nm}$ .

which is higher than that found measuring amorphous LSMO powder of the same composition,  $T_C \approx 305\text{ K}$  [23]. In (b), the results of MTGA in the temperature range  $300\text{ K} < T < 470\text{ K}$  are shown with an applied magnetic field of  $0.1\text{ T}$ . When the sample changes from the

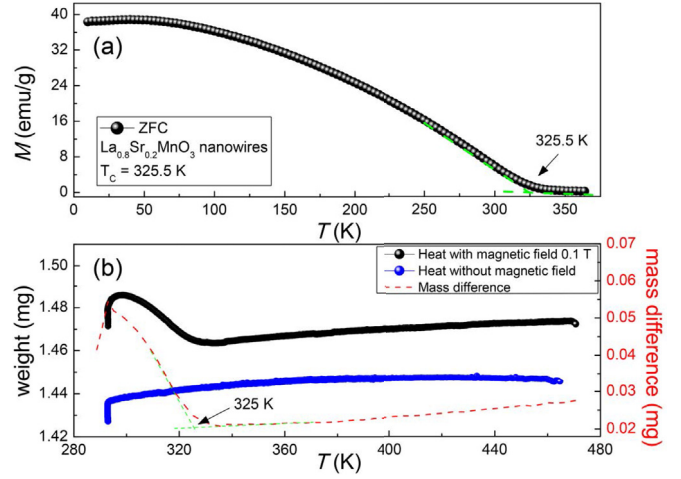


**Fig. 4.** (a):  $M(T)$  behavior in the temperature range  $2\text{ K} < T < 350\text{ K}$  measured using the SQUID magnetometer after zero-field cooling; (b): magnetic thermogravimetric analysis with (black curve) and without a field of  $0.1\text{ T}$  (blue curve). The dashed red line gives the difference between the two curves. The kink in this curve is an indication of the Curie temperature, determined to be  $325\text{ K}$ . (For interpretation of the references to colour in this figure legend, the reader is referred to the Web version of this article.)

paramagnetic to ferromagnetic state, the experienced magnetic force counteracts the gravity of the sample mass. Thus, using the mass difference between the curves with and without magnetic field,  $T_C$  can be estimated. From the resulting dashed red line, a kink is revealed at  $325\text{ K}$ , which corresponds to  $T_C$  obtained from the  $M(T)$  measurement (a).

**Fig. 5** presents the magnetization data obtained at  $10\text{ K}$  and  $300\text{ K}$ . The soft magnetic character of the LSMO sample is clearly revealed. The values of the saturation magnetization ( $M_s$ ) are  $52.12\text{ emu/g}$  at  $10\text{ K}$ , and  $18.10\text{ emu/g}$  at  $300\text{ K}$ . These values are lower than the ones from the corresponding bulk materials ( $56\text{ emu/g}$  [24]), which can be attributed to the smaller grain size of our nanowire network fabric samples.

Magnetoresistance (MR) plots are calculated from the resistance data obtained by sweep measurements at different field strengths using the relation  $\text{MR}[\%] = (R_H(T) - R_0(T))/R_0(T)$ . **Fig. 6** presents the resistance measurements and the MR ratio of the LSMO sample measured in applied fields up to  $10\text{ T}$  ( $H$  is applied perpendicular to the sample surface) in the temperature range from  $2\text{ K}$  to  $275\text{ K}$ . In (a),  $R$  vs.  $T$

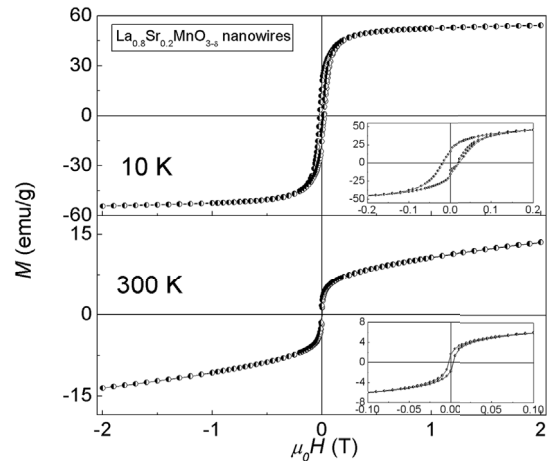


**Fig. 5.**  $M(H)$  measurement of the LSMO nanowires at  $T = 10\text{ K}$  and  $300\text{ K}$  for the LSMO nanowire network fabrics with  $x = 0.2$ . The insets present the low-field parts of the  $M(H)$  loops.

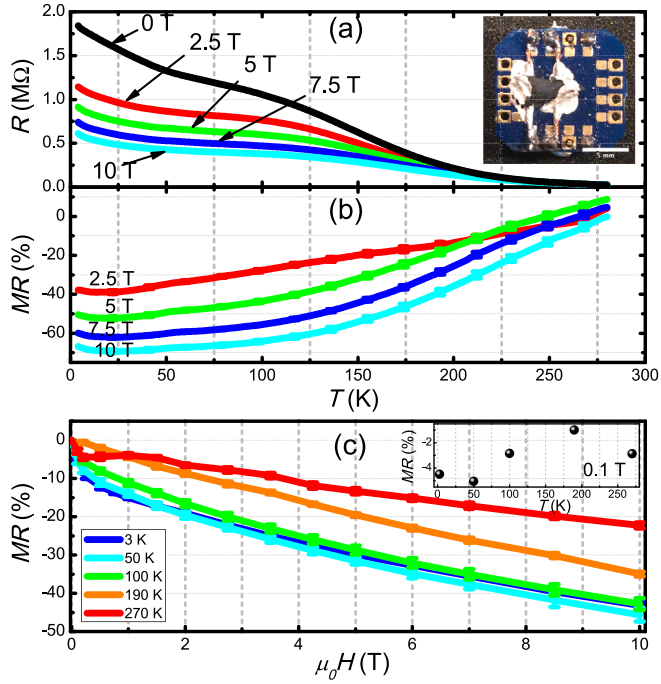


**Fig. 6.** Resistance (a) and MR ratio (b) of the LSMO nanowire network sample measured up to 10 T with applied magnetic fields ( $H \perp$  sample surface) in the range  $2\text{ K} < T < 275\text{ K}$ . The inset to (a) shows the sample with the electric connections mounted on the sample holder. (c) presents the MR ratio as function of the applied magnetic field for various temperatures. The inset to (c) gives the LFMR measured at 0.1 T as function of temperature.

curves are given with the inset showing the electric connections to the nanowire fabric sample. Fig. 6 (b) presents the MR vs.  $T$  curves from 0 to 10 T and (c) shows the MR ratio as a function of the applied magnetic field in the temperature range  $3\text{ K} < T < 270\text{ K}$ , with the inset graph presenting the LFMR at 0.1 T as function of temperature.

Three main features can be seen from Fig. 6: Firstly, there is a suppression of the metal-insulator transition. This provides another evidence of the size effect. Nanoscale grains are always accompanied by a large number of grain boundaries, which enhance electron scattering. By plotting the  $\log(\rho)-1/\sqrt{T}$  curve at 0 T as shown in Fig. 7, a linear behaviour is observed when  $T \leq 13\text{ K}$ , which means in this regime the resistivity follows the relationship  $\rho \sim \exp \sqrt{\delta/T}$ , with an activation energy  $\delta = 0.7\text{ meV}$ . This indicates that the anti-metallic behaviour at lower temperature may be attributed to the Coulomb blockade [2]. To confirm this argument, a calculation of the charging energy  $E_C$  is required.  $E_C$  can be defined via

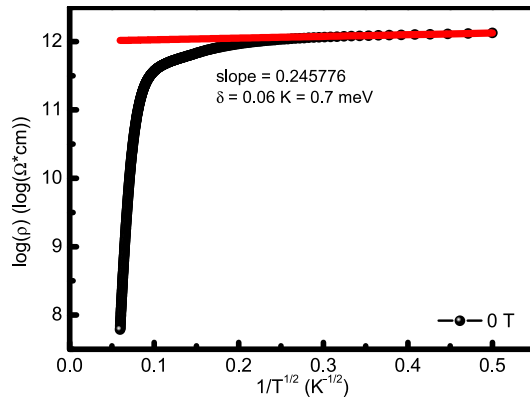


**Fig. 7.** Relationship of  $\log(\rho)$  on  $1/\sqrt{T}$  at 0 T. When  $T \leq 16\text{ K}$ ,  $\rho$  follows the  $\exp(\sqrt{\delta/T})$  behaviour, with the  $\delta$  value shown in the graph.

$$E_C = \left( \frac{e^2}{\pi \epsilon_0 \epsilon_d} \right) \left( \frac{s}{s + \frac{d}{2}} \right), \quad (1)$$

where  $\epsilon_0$  is the dielectric constant of the medium, which for the manganites is taken as 10 [7].  $\epsilon_d$  is a size-related parameter that  $\epsilon_d = d/s$ .  $d$  is the average grain size and  $s$  denotes the inter-particle separation. For the polycrystalline materials, the value of  $s$  can be chosen from the thickness of the grain boundary. In our case, the average grain size is 24.8 nm and the thickness of the grain boundary is about 5 nm according to the TEM observations. Then, we obtain  $E_C \approx 1.147\text{ meV} \approx 13.3\text{ K}$ . Since the temperature regime of the  $\rho \sim \exp \sqrt{\delta/T}$  behaviour is below 13 K, which is right lower than  $E_C$ , the contribution of the Coulomb blockage is confirmed. On the other hand, the influence from certain size effects varies with the doping level  $x$ . So, a step-shape resistance behavior can be observed for the  $x = 0.2$  sample, which indicates that the metal-insulator transition is not completely suppressed.

Secondly, at an external field of 0.1 T, a maximum MR of 5.05% is obtained at  $T = 50\text{ K}$  (see the inset to Fig. 6 (b)). Such value is not too high, however, it can otherwise only be achieved when mixing other compounds to the  $\text{La}_{0.8}\text{Sr}_{0.2}\text{MnO}_3$  powder [25], which can enhance the LFMR. This may point to the contribution of the interconnects of our nanowire fabric sample, which still needs to be further clarified. Jugdersuren et al. reported a large LFMR at room temperature in their LSMO nanowires extracted from the network fabrics produced by electrospinning and showed a dependence of the LFMR on the nanowire diameter, but no information on the LSMO grain size was presented [17]. However, the LFMR at 300 K for our complete network sample is comparable to their data, even though the chemical composition is somewhat different. Nevertheless, this demonstrates that the LFMR can be considerably enhanced by reducing the nanowire diameter as well as the LSMO grain size. This opens another possible path of LFMR enhancement besides adding other components. Thirdly, the sample exhibits a strong MR effect at low temperatures as shown in Fig. 8. At an applied field of 2.5 T, the maximum of the MR is already over 40%, while a MR ratio of nearly 70% is observed for the sample at 24.5 K and 10 T field, which confirms that the HFMR can be increased by reducing the grain size as reported by Balcells et al. [7,8]. In these works, a maximum HFMR of  $3.9 \times 10^{-6}\text{ Oe}^{-1}$  was obtained at 10 K and an applied field of 50 kOe for a sample with a grain size of 15 nm, while  $M_s$  was comparable to our sample. The reason for the large HFMR was ascribed to the interface area of the LSMO grains. In a recent work this assumption was confirmed by an investigation of cubic LSMO nanoparticles, which can be described as core-shell nanoparticles with a shell of about 1 nm thickness around the LSMO core [11]. Reducing the

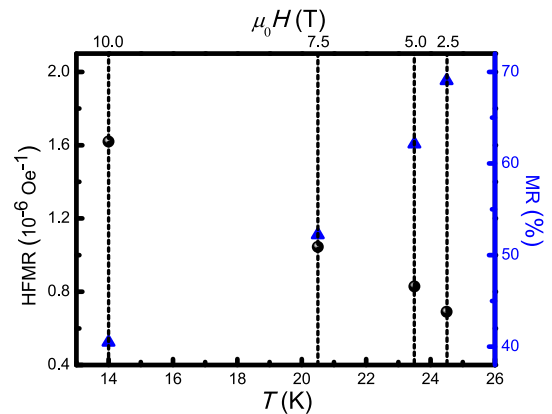


**Fig. 8.** Temperature dependence of the HFMR extracted from Fig. 6 (b). Each data point reaches the maximum MR at the corresponding temperature as shown on the blue triangle dots. (For interpretation of the references to colour in this figure legend, the reader is referred to the Web version of this article.)

LSMO grain size increases the importance of this shell layer, resulting in a larger HFMR.

#### 4. Conclusion

Non-woven nanowire networks of LSMO with  $x = 0.2$  were fabricated by means of the electrospinning technique. The magnetoresistance effect of these nanowire network fabrics was measured up to 10 T applied field at temperatures between 5 K and 300 K. The reduced dimensions of the nanowires (grain size, wire diameter) and the large number of interconnects between them were found to increase the MR effect as compared to bulk LSMO samples. A MR ratio of nearly 70% was observed for the sample  $x = 0.2$  at low temperatures and 10 T field.

#### Acknowledgment

We thank J. Schmauch (Saarland University, group Prof. Birringer) for technical assistance and Prof. V. Presser (Saarland University) for the use of the electrospinning apparatus. This work is supported by DFG grant Ko2323/8, which is gratefully acknowledged.

#### References

- [1] Y.N. Xia, P.D. Yang, Y.G. Sun, Y.Y. Wu, B. Mayers, B. Gates, Y.D. Yin, F. Kim, Y.Q. Yan, *Adv. Mater.* 15 (2003) 353.
- [2] T. Sarkar, M.V. Kamalakar, A.K. Raychaudhuri, *New J. Phys.* 14 (2012) 033026.
- [3] G.P. Dwivedi, M. Kumar, P. Shahi, A. Barman, S. Chatterjee, A.K. Ghosh, *RSC Adv.* 5 (2015) 30748.
- [4] H.Y. Hwang, S.-W. Cheong, N.P. Ong, P. Batlogg, *Phys. Rev. Lett.* 77 (1996) 2041.
- [5] X.W. Li, A. Gupta, G. Xiao, G.Q. Gong, *Appl. Phys. Lett.* 71 (1997) 1124.
- [6] A. Gupta, G.Q. Gong, G. Xiao, P.R. Duncombe, P. Lecoeur, P. Trouilloud, Y.Y. Wang, V.P. Dravid, J.Z. Sun, *Phys. Rev. B* 54 (1996) R15629.
- [7] Ll. Balcells, J. Fontcuberta, B. Martinez, X. Obradors, *Phys. Rev. B* 58 (1998) R14697.
- [8] Ll. Balcells, B. Martinez, F. Sandiumenge, J. Fontcuberta, *J. Magn. Magn. Mater.* 211 (2000) 193.
- [9] J. Fontcuberta, B. Martinez, V. Laukhin, Ll. Balcells, X. Obradors, C.H. Cohenca, R. Jardim, *Philos. Trans. R. Soc. London, Ser. A* 356 (1998) 1577.
- [10] J.-H. Park, E. Vescovo, H.-J. Kim, C. Kwon, R. Ramesh, T. Venkatesan, *Phys. Rev. Lett.* 81 (1998) 1953.
- [11] Ha Le Thi N'Goc, L.D. Notemngnou Mouafo, C. Etrillard, A. Torres-Pardo, J.-F. Dayen, S. Rano, G. Rousse, C. Laberty-Robert, J. Gonzales Calbet, M. Drillon, C. Sanchez, B. Doudin, D. Portehault, *Adv. Mater.* 29 (2017) 1604745.
- [12] D. Li, J.T. McCann, Y.N. Xia, *J. Am. Ceram. Soc.* 89 (2006) 1861.
- [13] H. Wu, W. Pan, D. Lin, H. Li, *J. Adv. Ceram.* 1 (2012) 2.
- [14] D. Li, T. Herricks, Y.N. Xia, *Appl. Phys. Lett.* 83 (2003) 4586.
- [15] Y. Liu, X. Sun, B. Li, Y. Lei, *J. Mater. Chem.* 2 (2014) 11651.
- [16] J. Zheng, K. Du, D. Xiao, Z.-Y. Zhou, W.G. Wei, J.J. Chen, L.F. Yin, *J. Shen, Chin. Phys. Lett.* 33 (2016) 097501.
- [17] B. Jugdersuren, S. Kang, R.S. Di Pietro, D. Heiman, D. McKeown, I.L. Pegg, *J. Appl. Phys.* 109 (2011) 016109.
- [18] R. Yensano, S. Pinitsoontorn, V. Amornkitbamrung, S. Maensiri, *J. Supercond. Nov. Magnetism* 27 (2014) 1553.
- [19] D. Pesquera, G. Herranz, A. Barla, E. Pellegrin, F. Bondino, E. Magnano, F. Sanchez, J. Fontcuberta, *Nat. Commun.* 3 (2012) 542.
- [20] P.K. Muduli, S.K. Bose, R.C. Budhani, *J. Phys. Condens. Matter* 19 (2007) 226024.
- [21] J.-M. Li, X.L. Zeng, A.-D. Moe, Z.-A. Xu, *CrystEngComm* 13 (2011) 6964.
- [22] X.L. Zeng, M.R. Koblischka, U. Hartmann, *Mater. Res. Express* 2 (2015) 095022.
- [23] D.L. Rocco, R. Almeida Silva, A. Magnus, G. Carvalho, A.A. Coelho, J.P. Andreetta, S. Gama, *J. Appl. Phys.* 97 (2005) 10M317.
- [24] M. Dominiczak, A. Ruyter, P. Limelette, I.M. Laffez, F. Giovannelli, M.D. Rossell, G.V. Tendeloo, *Solid State Commun.* 149 (2009) 1543.
- [25] W.J. Lu, Y.P. Sun, X.B. Zhu, W.H. Song, J.J. Du, *Mater. Lett.* 60 (2006) 3207.